Journal of Molecular Liquids 252 (2018) 169–179

Contents lists available at ScienceDirect

Journal of Molecular Liquids

journal homepage: www.elsevier.com/locate/molliq

Colloidal study of unsteady magnetohydrodynamic couple stress fluid flow over an isothermal vertical flat plate with entropy heat generation

G. Janardhana Reddy [a], Mahesh Kumar [a], Bhaskerreddy Kethireddy [a], Ali J. Chamkha [b,c,*]

[a] Department of Mathematics, Central University of Karnataka, Kalaburagi 585367, India
[b] Mechanical Engineering Department, Prince Mohammad Bin Fahd University, Al-Khobar 31952, Saudi Arabia
[c] RAK Research and Innovation Center, American University of Ras Al Khaimah, United Arab Emirates

ARTICLE INFO

Article history:
Received 8 September 2017
Received in revised form 13 November 2017
Accepted 20 December 2017
Available online 22 December 2017

Keywords:
Couple stress fluid
Entropy generation
Bejan number
Vertical plate
Heat transfer
Finite difference method

ABSTRACT

The present work aims to examine the entropy heat generation analysis for unsteady MHD couple stress fluid flow over a uniformly heated vertical flat plate. The mathematical model of this problem is given by highly time reliant non-linear coupled equations and resolved by an efficient unconditionally stable implicit scheme. The time histories of average values of momentum and heat transport coefficients, entropy and Bejan lines, as well as the steady-state flow variables, discussed for several values of non-dimensional parameters arising in the flow equations. Results specify that time required to attain the time independent flow with respect to the flow field variables get amplified with the augmented values of couple stress parameter. The outcomes also indicate that entropy generation parameter upsurges with rising values of group parameter and Grashof number while the reverse trend is observed for couple stress parameter and magnetic parameter.

1. Introduction

The analysis of the flow past a vertical plate with boundary layer theory is interested primarily in the drag force and the nature of the flow pattern, which include several applications such as heat exchangers, in the glass and polymer industries, cooling systems, electronic equipment, aerodynamic extrusion of plastic sheets, etc.

Studies on non-Newtonian fluids with convective heat transfer have many applications in science and engineering. These fluids are demarcated by a non-linear constitutive correlation between the strain and the stress. Various mathematical models have existed and explained the behaviour of non-Newtonian relationship from that of the Newtonian fluids. Non-Newtonian fluids, for example polymers, pulps, molten plastics, milk, jelly, ink, glues, mayonnaise, slurries, hand cream, foodstuffs etc. are progressively used in numerous manufacturing and engineering applications particularly in the industries such as cosmetics, pharmaceuticals, chemicals, polymer processing and biotechnology. These non-Newtonian fluids under free convective flow have garnered substantial attention by many researchers. The first study of laminar natural convection heat transfer problem from an isothermal vertical plate to a non-Newtonian fluid was presented by Acrivos [1]. In particular substantial attention has been given to the non-Newtonian fluid flow past vertical flat plate problems in the literature. Some attempts have also been made for transient convection on vertical plate with various aspects (see refs [2–6].). Due to numerous rheological features of non-Newtonian fluid models, they are given importance in the literature. One such non Newtonian fluid is couple stress fluid given by Stokes [7]. These fluids have various features such as body couples, couple stresses, and non-symmetric stress tensor. The study of these fluids have applications in lubrication theory [8], blood flow [9], squeeze film [10], Bio-fluid mechanics [11] and in the bearing system [12]. Also it has several industrial applications such as thickened oils, synthetic fluid, colloidal solutions, freezing of metallic plate in a bath, etc. Devakar and Iyengar [13] studied the couple stress fluid problem between two parallel plates with the concept of run up of flow. Khan et al. [14] analyzed the heat transfer couple stress fluid flow past stretching sheet. Recently, Akhtar [15] studied the transient flow between parallel plates with two different time-fractional derivatives for couple stress fluid.

Recent years have seen wide interest in the subject of magnetohydrodynamics (MHD). This area of study is concerned with the motions of fluids which possess an electrical conductivity in the presence of electric and magnetic fields. The motion of an electrically conducting fluid in a magnetic field generates induced electric currents which interact with the original magnetic field and yield mechanical forces which alter the fluid motion. Various scientific endeavours today are concerned with the phenomena associated with MHD: controlled thermonuclear fusion research and high speed aerodynamics, in flow control, communications, aerodynamics, plasma containment, propulsion and power generation, electrical components transmission lines, forming metal etc. The

* Corresponding author.
E-mail address: achamkha@pmu.edu.sa (A.J. Chamkha).

https://doi.org/10.1016/j.molliq.2017.12.106
0167-7322/

Nomenclature

B_0	applied magnetic field
Be	dimensionless Bejan number
B	magnetic flux
Br	Brinkman number
c_p	specific heat at constant pressure
$\bar{C}_f$	dimensionless average momentum transport coefficient
d_{ij}	rate of deformation tensor
E	electric field
g	acceleration due to gravity
Gr	Grashof number
H	magnetic field
J	current density
k	thermal conductivity
Ns	dimensionless entropy heat generation number
$\bar{N}u$	dimensionless average heat transport coefficient
M	magnetic field parameter
m	trace of couple stress tensor
m_{ij}	couple stress tensor
Pr	Prandtl number
p	fluid pressure
q	velocity vector
t′	time
t	dimensionless time
T′	temperature
T	dimensionless temperature
τ_{ij}	force stress tensor
x	axial coordinate
y	transverse coordinate
u, v	velocity components in (x, y) coordinate system
X	dimensionless axial coordinate
Y	dimensionless transverse coordinate
U, V	dimensionless velocity components in *X*, *Y* directions, respectively

Greek letters

η	material constant
β	couple stress fluid parameter
η, η'	couple stress viscosity coefficients
β_T	volumetric coefficient of thermal expansion
α	thermal diffusivity
ρ	density
μ, λ	viscosity coefficients
ν	kinematic viscosity
ε_{ijk}	Levi-Civita symbol
ω	spin vector
ω_{ij}	spin tensor
σ	electrical conductivity of the fluid
Ω	dimensionless temperature difference
$\mathrm{Br}\Omega^{-1}$	dimensionless group parameter
δ_{ij}	Kronecker delta

Subscripts

l, *m*	grid levels in (X, Y) coordinate system
w	wall conditions
∞	ambient conditions

Superscripts

n	time level

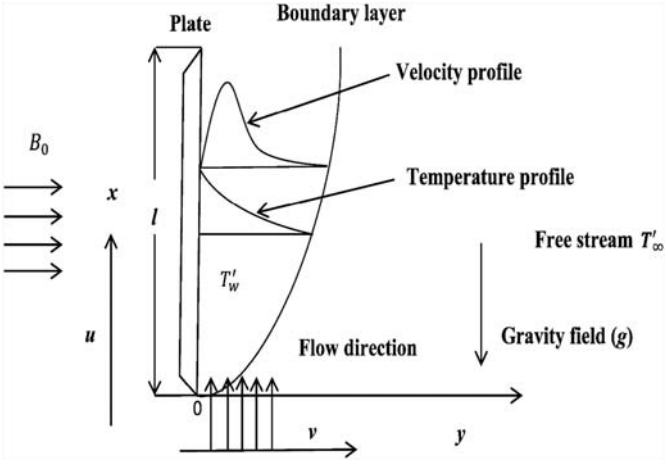

Fig. 1. Flow geometry and coordinate system.

application of magnetohydrodynamics play vital role in the blood flow [16], plasma technology [17], direct numerical simulations [18], seawater propulsion [19], drag reductions in the boundary layer [20], and other recent applications can be found in [21–22]. Few works on MHD couple stress fluid flow for various configurations have been found in [23–25]. Recently, Srinivasacharya and Madhava Rao [26] examined the MHD effect for pulsatile flow of couple stress through the artery. Khan et al. [27] examined the MHD flow problem for couple stress fluid with heat transfer. Ali et al. [28] presented the MHD flow of couple stress fluid past a sheet.

The laws of thermodynamics and Newton's second law of motion are the basic principles on which all the flow and heat transfer systems developed today. First law of thermodynamics provides information about the energy of the system quantitatively. On the other hand, the second law of thermodynamics states that entire actuality processes are irretrievable and it is a useful tool to examine the entropy generation to assess the irreversibility in the system. Entropy production determines the irreversibility related to the natural processes such as a counter flow heat exchange for gas to gas applications. Currently, entropy analysis was the subject of various interests in several areas comparable to turbo machinery, rotating disk reactors, porous media, electric cooling, heat transferring devices, electromagnetic materials processing and propulsion ducts, and combustions. Few recent applications of entropy generation are pseudo-optimization design process in solar heat exchangers [29], minimizing lost available work during heat transfer processes [30] and multifield flows [31]. The foremost of the energy-related applications, for example, cooling of nuclear fuel rods, nuclear swirl electromagnetic propulsion, slurry systems, heat loss from steam pipes, cooling of modern electronic systems, solar energy collectors, and heat energy systems rely on entropy generation. The study of entropy generation with a magnetohydrodynamic flow has received considerable attention due to ever-growing applications such as MHD generators, micropumps, power plant, nuclear reactors, accelerators, flow meters, filtration and geothermal systems etc. Furthermore, the study of entropy generation for hydromagnetic couple stress fluid flow has significant applications such as designing porous lining [32], analysing channel flow [33,34], etc. Several researchers studied the

Table 1
Grid independence test for selecting mesh size.

Grid size	Average Nusselt number $(\overline{Nu})$ for $Pr = 0.71, \beta = 0.2, M = 1.0$
25 × 125	0.35100727
50 × 250	0.35533096
100 × 500	0.35954117
200 × 1000	0.35959198

Table 2
Grid independence test for selecting time step size.

Time step size (Δt)	Average Nusselt number ($\overline{Nu}$) for $Pr = 0.71, \beta = 0.2, M = 1.0$
0.5	0.35954305
0.1	0.35953980
0.08	0.35953980
0.05	0.35953962
0.02	0.35954043
0.01	0.35954117

entropy generation concept related to the heat transfer problem for different geometries. Ramana Murthy and Srinivas [35] analyzed the first and second law of thermodynamic for MHD flow of couple stress fluid between parallel plates. Aksoy [36] studied the influence of couple stress fluid on entropy generation between parallel plates. Recently, Srinivas et al. [37] analyzed the entropy generation in flow of two immiscible incompressible couple stress fluids between two horizontal parallel plates.

From the previous studies, it is observed that very scant attention has been paid for the time-dependent couple stress fluid flow past a vertical flat plate along with entropy heat generation. Thus, it is focused to analyze the second law of thermodynamic analysis for couple stress fluid flow over a uniformly heated vertical flat plate in the boundary layer region. The temperature at the surface is taken to be greater than that of surrounding fluid temperature. The governing equations of couple stress fluid are complicated, coupled, non-linear and higher-order compared with those of Navier-Stokes equations. Thus, in general, one can obtain the numerical results by applying the implicit finite difference method and are corroborated with the previously published results available in the literature. The transient assets of the couple stress fluid flow with entropy heat generation are studied for the momentum and heat transport coefficients for different control parameters and compared with the Newtonian fluid flow.

2. Problem description

Transient two-dimensional laminar buoyancy driven couple stress fluid flow past a semi-infinite vertical plate of length l with transversely applied magnetic field B_0, which is aligned vertically is considered and described in Fig. 1. The rectangular coordinate system is chosen, in which the axial coordinate (x-axis) is selected vertically upward direction of the plate, while the transverse coordinate (y-axis) is assessed normal to the plate at the foremost edge. The neighbouring fluid temperature is considered to be stationary and similar to that of free stream temperature T_∞'. At the outset, i.e. $t' = 0$, the temperature T_∞' is uniform for the plate and surrounding fluid. Later ($t' > 0$), the temperature of the vertical plate is augmented to T_w' ($> T_\infty'$) and preserved uniformly there afterward. The influence of viscous dissipation is presumed to be insignificant in the thermal equation, since the fact that, in the flow region, the magnitude of velocity is expected to be minuscule. The incompressible couple stress fluid is modelled by the following constitutive equations:

Law of conservation of mass:

$$\frac{\partial u}{\partial x} + \frac{\partial v}{\partial y} = 0 \tag{1}$$

Law of conservation of momentum:

$$\rho\left[\frac{\partial \mathbf{q}}{\partial t'} + (\mathbf{q}.\nabla)\mathbf{q}\right] = -\rho g - \nabla p + \mu\nabla^2\mathbf{q} - \eta\nabla^4\mathbf{q} + (\mathbf{J}\times\mathbf{B}) \tag{2}$$

where, **J** and **B** are given by Ohm's law and Maxwell's equations, namely,

$$\nabla\times\mathbf{E} = 0,\ \ \nabla\times\mathbf{H} = 4\pi\mathbf{J},\ \ \nabla\times\mathbf{B} = 0,\ \ \mathbf{J} = \sigma[\mathbf{E} + \mathbf{q}\times\mathbf{B}]$$

Here, **J** - current density, **E** - electric field, **H** - magnetic field, **B** - magnetic flux, **q** - velocity vector and σ - the electrical conductivity of the fluid. The considered plate is under the effect of a transverse magnetic field with a uniform strength, B_0, as shown in Fig. 1. It is presumed that the magnetic Reynolds number is very small. Therefore, the interaction of the induced axial magnetic field with the motion of electrically-conducting couple stress fluid flow is expected to be minuscule compared to the interaction of the applied magnetic field. Further, no external electric field is applied. With these assumptions, the magnetic field $\mathbf{J}\times\mathbf{B}$ of the body force term in momentum Eq. (2) reduces to $-\sigma B_0^2 u$ where B_0 is the intensity of the forced transverse magnetic field. Here, it is assumed that the vertical scale of the flow is too small so that the hydrostatic pressure variations cannot cause the significant changes in the density. Under these circumstances, the Boussinesq's approximation is relevant to the couple stress fluid [38]. Using Boussinesq's approximation, Eq. (2) can be rewritten as [7,38,39,40]

$$\rho\left(\frac{\partial u}{\partial t'} + u\frac{\partial u}{\partial x} + v\frac{\partial u}{\partial y}\right) = g\beta_T(T' - T_\infty') + \mu\frac{\partial^2 u}{\partial y^2} - \eta\frac{\partial^4 u}{\partial y^4} - \sigma B_0^2 u \tag{3}$$

Law of conservation of energy:

$$\frac{\partial T'}{\partial t'} + u\frac{\partial T'}{\partial x} + v\frac{\partial T'}{\partial y} = \alpha\frac{\partial^2 T'}{\partial y^2} \tag{4}$$

The stress tensors related to couple stress fluid theory is given by [7, 39]

$$\tau_{ij} = (-p + \lambda\nabla.\mathbf{q})\delta_{ij} + 2\mu d_{ij} - \frac{1}{2}\varepsilon_{ijk}\left[m_{,k} + 4\eta\omega_{k,rr} + \rho c_k\right] \tag{5}$$

$$m_{ij} = \frac{1}{3}m\delta_{ij} + 4\eta'\omega_{j,i} + 4\eta\omega_{i,j} \tag{6}$$

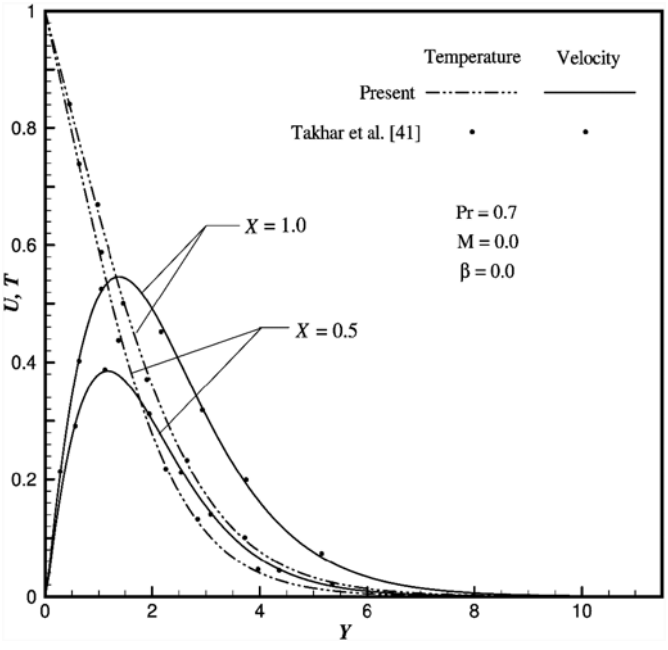

Fig. 2. Comparison of flow-field variables.

In the above Eqs. (5)–(6) $p, \tau_{ij}, d_{ij}, \delta_{ij}, \omega_{j,i}, \varepsilon_{ijk}, \rho c_k$ represents the fluid pressure, force stress tensor, rate of deformation tensor, Kronecker delta, spin tensor, Levi-Civita symbol (permutation symbol) and body couple vector respectively. $m\ (=m_{11}+m_{22}+m_{33})$, $\omega(=\frac{1}{2}\nabla\times\mathbf{q})$ denotes the trace of a couple stress tensor m_{ij} and spin vector respectively. Comma in the suffixes denotes covariant differentiation and $\omega_{k,rr}$ stands for $\omega_{k,11}+\omega_{k,22}+\omega_{k,33}$.

The viscosity coefficients λ, μ and the couple stress viscosity coefficients η, η' are the material constants and which constrained by the following relation.

$$3\lambda+2\mu\geq 0;\ \mu\geq 0;\ |\eta'|\leq\eta;\ \eta\geq 0 \tag{7}$$

The distinctive measure of the polarity of the fluid model is a length parameter $l(=\sqrt{\frac{\eta}{\mu}})$ [39], and this parameter is identically zero in the case of non-polar fluids.

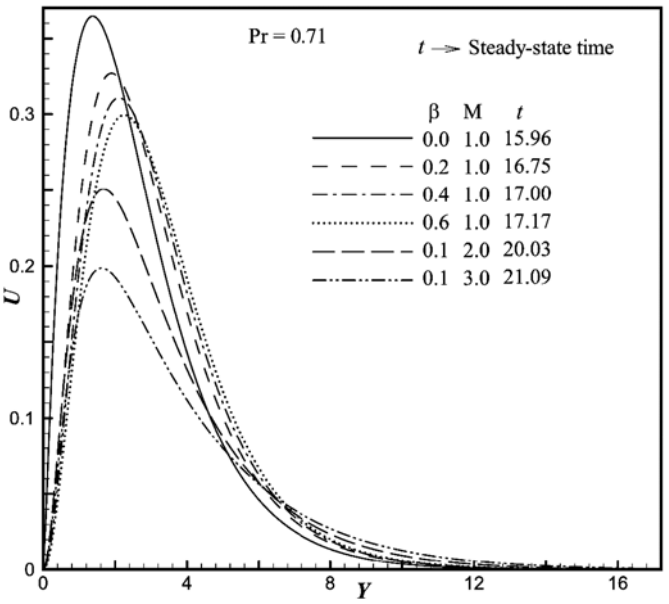

Fig. 4. Simulated time-independent state velocity profile (U) versus Y at $X = 1.0$ for various values of β and M.

The resultant initial and boundary conditions are given by

$$\begin{aligned} &t'\leq 0: T'=T'_{\infty}, u=0, v=0 \quad \text{for all } x \text{ and } y\\ &t'>0: T'=T'_{w}\ , u=0, v=0 \qquad \text{at } y=0\\ &T'=T'_{\infty}, u=0, v=0 \qquad\qquad \text{at } x=0\\ &T'\to T'_{\infty},\ \ u\to 0, v\to 0 \qquad \text{as } y\to\infty \end{aligned} \tag{8}$$

For the flow of couple stress fluid, V. K. Stokes [39] suggested that the vorticity of the fluid on the boundary is equal to the rotational velocity

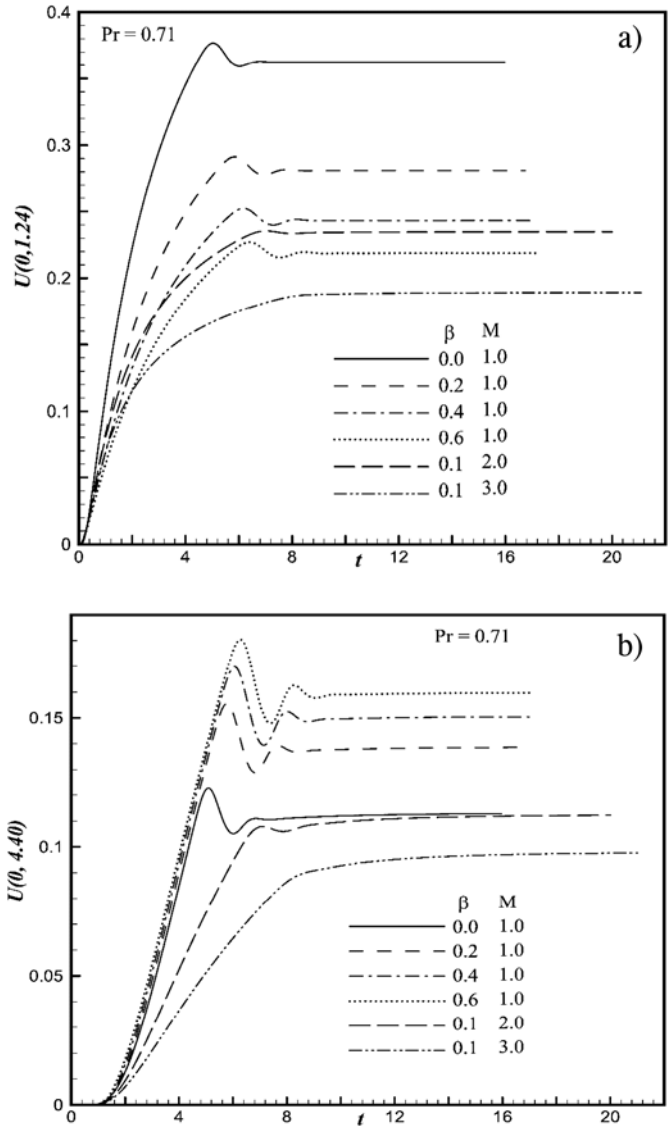

Fig. 3. Time-dependent velocity profile (U) versus time (t) for various values of β and M at the location (a) (0, 1.24); & (b) (0, 4.40).

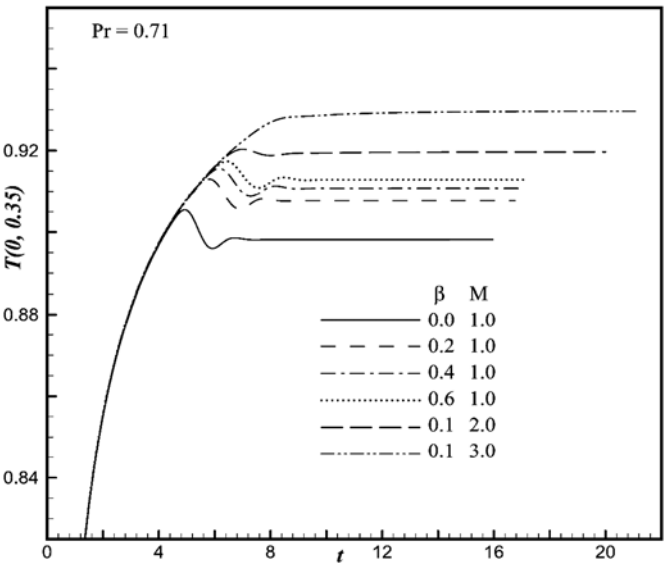

Fig. 5. Simulated time-dependent temperature profile (T) versus time (t) at the location (0, 0.35) for distinct values of β and M.

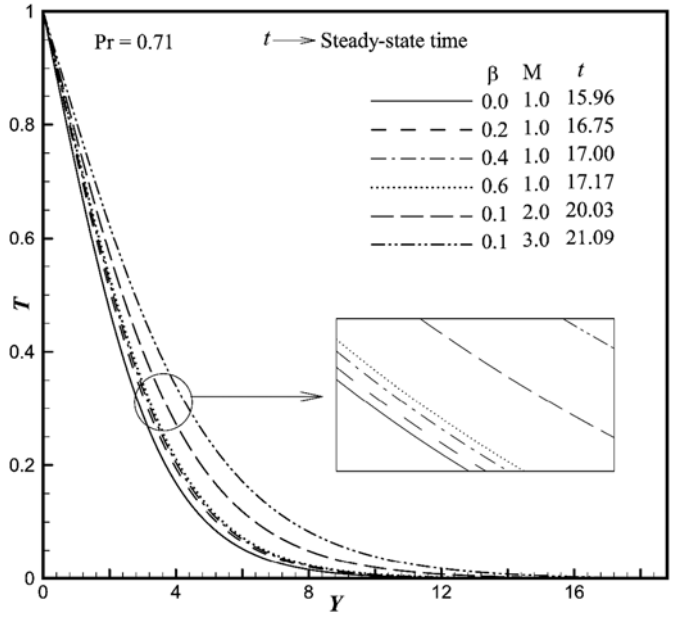

Fig. 6. Simulated time-independent temperature profile (T) versus Y at $X = 1.0$ for various values of β and M.

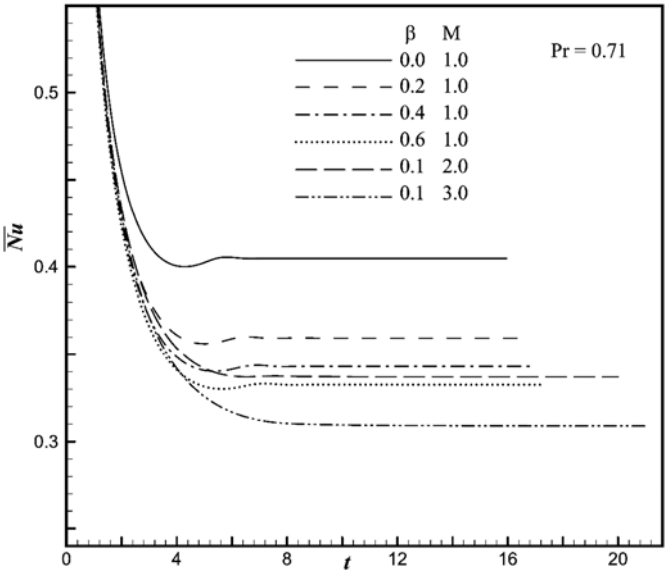

Fig. 8. Average heat transport coefficient ($\overline{Nu}$) for different values of of β and M.

of the boundary, i.e., Curl $\mathbf{q} = 0$

$$\Rightarrow \frac{\partial u}{\partial y} = \frac{\partial v}{\partial x} \text{ at } y = 0 \text{ and as } y \to \infty \tag{9}$$

where $\mathbf{q}$ is the velocity vector.

Now, initiating the subsequent non-dimensional quantities (for the below symbols refer nomenclature)

$$X = \mathrm{Gr}^{-1}\frac{x}{l}, Y = \frac{y}{l},\ U = \mathrm{Gr}^{-1}\frac{ul}{\upsilon},\ V = \frac{vl}{\upsilon}, t = \frac{\upsilon t'}{l^2}, T = \frac{T' - T'_\infty}{T'_w - T'_\infty}, \mathrm{Gr} = \frac{g\beta_T l^3 (T'_w - T'_\infty)}{\upsilon^2},$$

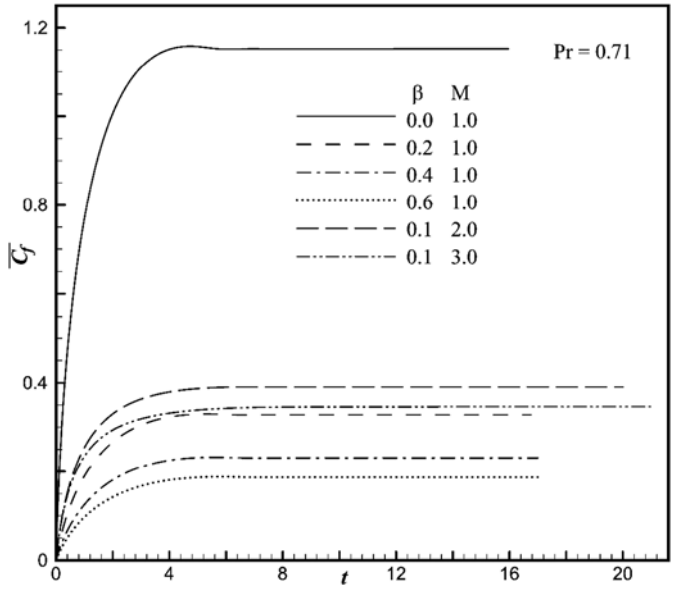

Fig. 7. Average momentum transport coefficient ($\overline{C_f}$) for different values of β and M.

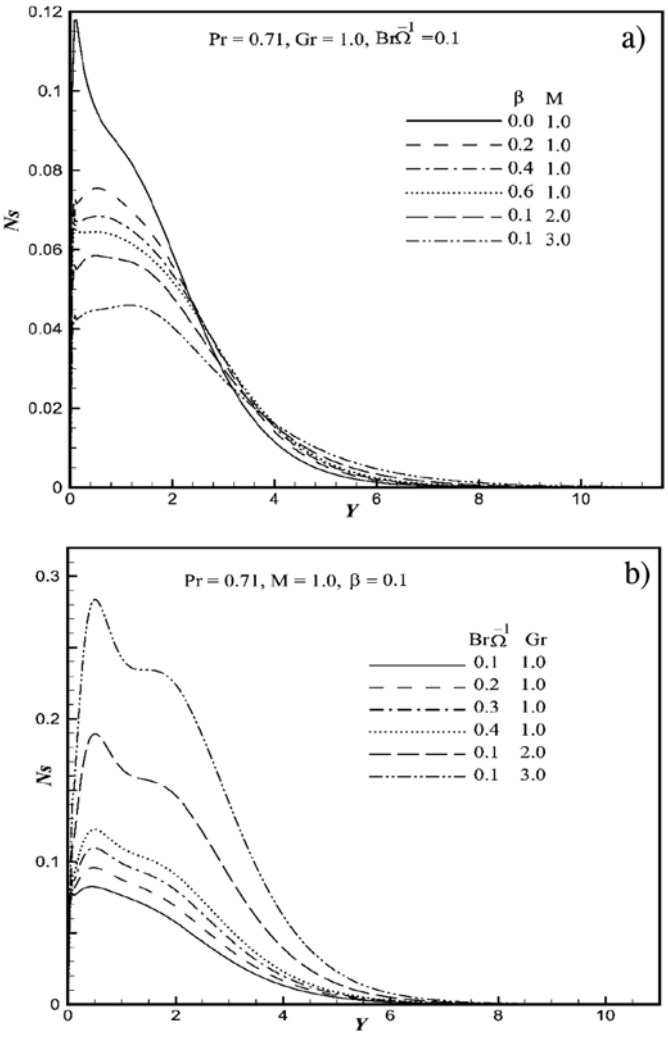

Fig. 9. Simulated steady-state entropy profile (Ns) versus Y at $X = 1.0$ for different values of (a) β and M; & (b) $\mathrm{Br}\Omega^{-1}$ and Gr.

$$\mathrm{Pr}=\frac{\upsilon}{\alpha},\mathrm{Br}=\frac{\mu\upsilon^2}{k(T'_w-T'_\infty)l^2},\Omega=\frac{(T'_w-T'_\infty)}{T'_\infty},\mathrm{M}=\frac{\sigma B_0^2 l^2}{\rho\upsilon},\beta=\frac{\eta}{\mu l^2}$$

in the Eqs. (1), (3), (4), (8) and also in Eq. (9), they reduce to subsequent form:

$$\frac{\partial U}{\partial X}+\frac{\partial V}{\partial Y}=0 \tag{10}$$

$$\frac{\partial U}{\partial t}+U\frac{\partial U}{\partial X}+V\frac{\partial U}{\partial Y}=T+\frac{\partial^2 U}{\partial Y^2}-\beta\frac{\partial^4 U}{\partial Y^4}-\mathrm{M}U \tag{11}$$

$$\frac{\partial T}{\partial t}+U\frac{\partial T}{\partial X}+V\frac{\partial T}{\partial Y}=\frac{1}{\mathrm{Pr}}\frac{\partial^2 T}{\partial Y^2} \tag{12}$$

The initial and boundary conditions in non-dimensional form become

$$\begin{array}{ll} t\le 0: T=0, U=0, V=0 & \text{for all } X \text{ and } Y \\ t>0: \quad T=1, \ U=0, \ V=0 & \text{at } Y=0 \\ T=0, \ U=0, V=0 & \text{at } X=0 \\ T\to 0, \ U\to 0, \ V\to 0 & \text{as } Y\to\infty \end{array} \tag{13}$$

$$\frac{\partial U}{\partial Y}=\frac{\partial V}{\partial X} \text{ at } Y=0 \text{ and } Y\to\infty \tag{14}$$

3. Finite difference solution

To elucidate the above governing time-dependent mathematical flow-field Eqs. (10)–(12) along with initial and boundary conditions Eq. (13), an unconditionally stable finite difference iteration scheme such as Crank-Nicolson method is applied. The finite difference equations to the above Eqs. (10), (11) and (12) are as follows:

$$\frac{U_{l,m}^{n+1}-U_{l-1,m}^{n+1}+U_{l,m}^{n}-U_{l-1,m}^{n}}{2\Delta X}+\frac{V_{l,m}^{n+1}-V_{l,m-1}^{n+1}+V_{l,m}^{n}-V_{l,m-1}^{n}}{2\Delta Y}=0 \tag{15}$$

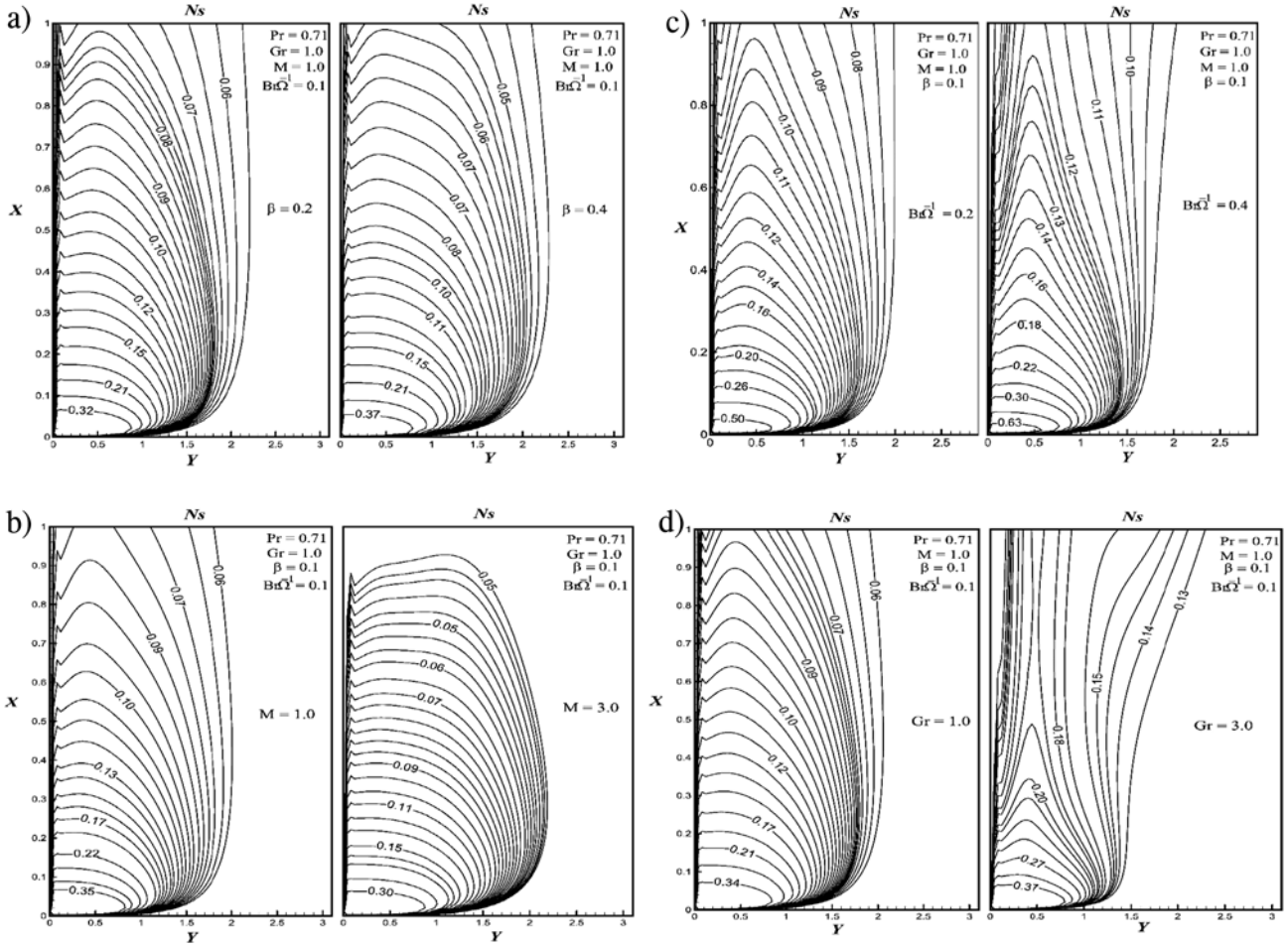

Fig. 10. Simulated steady-state entropy lines (*Ns*) for different values of (a) β; (b) $\mathrm{Br}\Omega^{-1}$; (c) M; & (d) *Gr*.

$$\frac{U_{l,m}^{n+1}-U_{l,m}^{n}}{\Delta t}+\frac{U_{l,m}^{n}}{2\Delta X}\left(U_{l,m}^{n+1}-U_{l-1,m}^{n+1}+U_{l,m}^{n}-U_{l-1,m}^{n}\right)+\frac{V_{l,m}^{n}}{4\Delta Y}\left(U_{l,m+1}^{n+1}-U_{l,m-1}^{n+1}+U_{l,m+1}^{n}-U_{l,m-1}^{n}\right)$$
$$=\frac{\mathrm{T}_{l,m}^{n+1}+\mathrm{T}_{l,m}^{n}}{2}+\left(\frac{U_{l,m+1}^{n+1}-2U_{l,m}^{n+1}+U_{l,m-1}^{n+1}+U_{l,m+1}^{n}-2U_{l,m}^{n}+U_{l,m-1}^{n}}{2(\Delta Y)^{2}}\right)$$
$$-\beta\left(\frac{U_{l,m+2}^{n+1}-4U_{l,m+1}^{n+1}+6U_{l,m}^{n+1}-4U_{l,m-1}^{n+1}+U_{l,m-2}^{n+1}+U_{l,m+2}^{n}-4U_{l,m+1}^{n}+6U_{l,m}^{n}-4U_{l,m-1}^{n}+U_{l,m-2}^{n}}{2(\Delta Y)^{4}}\right)-\mathrm{M}\left(\frac{U_{l,m}^{n}+U_{l,m}^{n+1}}{2}\right) \tag{16}$$

$$\frac{\mathrm{T}_{l,m}^{n+1}-\mathrm{T}_{l,m}^{n}}{\Delta t}+\frac{U_{l,m}^{n}}{2\Delta X}\left(\mathrm{T}_{l,m}^{n+1}-\mathrm{T}_{l-1,m}^{n+1}+\mathrm{T}_{l,m}^{n}-\mathrm{T}_{l-1,m}^{n}\right)+\frac{V_{l,m}^{n}}{4\Delta Y}\left(\mathrm{T}_{l,m+1}^{n+1}-\mathrm{T}_{l-1,m}^{n+1}+\mathrm{T}_{l,m+1}^{n}-\mathrm{T}_{l-1,m}^{n}\right)$$
$$=\left[\frac{\mathrm{T}_{l,m+1}^{n+1}-2\mathrm{T}_{l,m}^{n+1}+\mathrm{T}_{l,m-1}^{n+1}+\mathrm{T}_{l,m+1}^{n}-2\mathrm{T}_{l,m}^{n}+\mathrm{T}_{l,m-1}^{n}}{2\,Pr(\Delta Y)^{2}}\right]+\left[\frac{\mathrm{T}_{l,m+1}^{n+1}-\mathrm{T}_{l,m-1}^{n+1}+\mathrm{T}_{l,m+1}^{n}-\mathrm{T}_{l,m-1}^{n}}{4\,Pr(\Delta Y)}\right] \tag{17}$$

In the above Eqs. (15), (16) and (17) the subscripts l and m denote the grid points along the X and Y coordinates, respectively, where $X = l\Delta X$ and $Y = m\Delta Y$ and the superscript n designates a value of the time $t(=n\Delta t)$ with ΔX, ΔY and Δt the mesh sizes in the X, Y and t axes, respectively.

The results of these finite difference equations obtained in the rectangular grid with $X_{max} = 1$, $X_{min} = 0$, $Y_{max} = 20$ and $Y_{min} = 0$, where Y_{max} relates to $Y = \infty$ which lies far away from the heat and momentum transport boundary layers.

Validation of the numerical code using grid independence study

To have an economical consistent grid scheme for the reckonings, a grid independency test has been conducted using four different grid sizes of 25×125, 50×250, 100×500 and 200×1000 and the values of the average Nusselt number for the control parameters $Pr = 0.71$, $\beta = 0.2$ and $M = 1.0$ on the boundary $Y = 0$ is shown in Table 1. Regular grid is used for all cases. It is observed from Table 1 that 100×500 grid compared with 50×250 and 200×1000 does not have significant effect on the results of average Nusselt number. Hence according to this observation, a uniform grid size of 100×500 is enough for this study with the mesh sizes of 0.01 and 0.04 in axial and transverse directions, respectively. Similarly, to produce a reliable result with respect to time, a grid independent test has been done for different time step sizes is shown in Table 2 and the time step size Δt ($t = n\Delta t, n = 0,1,2,\ldots$) is fixed as 0.01.

4. Results and discussion

To study the unsteady behaviour of the virtual flow-field variables, such as temperature and velocity, their values are illustrated at different positions, which are neighbouring to the vertical plate.

The computer-generated flow-field profiles for the case of Newtonian fluids ($\beta = 0.0$) are similar with those of Takhar et al. [41] for $Pr = 0.7$ & $M = 0.0$, and are illustrated in Fig. 2. The outcomes are found to be in good covenant. These results confirm the validity and accurateness of the current numerical scheme. The simulated results are represented to describe the variation of the dimensionless flow variables, entropy generation number (Ns) and Bejan number (Be) which are examined along with average skin-friction and heat transport coefficients for different control parameters arise in this problem. Such variations are plotted and conferred in the following subsections.

4.1. Velocity

The simulated unsteady velocity (U) against time (t) at (0, 1.24) and (0, 4.40) locations for distinct values of couple stress parameter (β) and magnetic parameter (M) is graphically presented in Fig. 3. The U profiles, in Fig. 3(a) and (b), are taken in the vicinity and far away from the vertical plate, respectively. At all positions, the velocity curves augment with time, attains the temporal peak, then marginally decreases, and finally, they become independent of time. From Fig. 3(a) it is seen that in the vicinity of the vertical plate the transient U profile decreases with the increasing values β with fixed $M = 1.0$ and the reverse trend is noticed in the Fig. 3(b). Also, in the vicinity and far away from the vertical plate, the transient U curves decreases for all values of M with a fixed value of $\beta = 0.1$. The incentive behind for this decrement is that, as M increases, results in the decreasing of fluid viscosity, which is accountable in the reduction of the velocity profile. From the Fig. 3(a) and (b), it is noted that the time to attain the temporal peak upsurges as β amplifies. It is also noticed that from Fig. 3(a) the transient velocity of a Newtonian fluid ($\beta = 0$) is greater than the non-Newtonian couple stress fluid ($\beta > 0$) and the reverse trend is observed in Fig. 3(b). Therefore the unsteady velocity results corresponding to the couple stress fluid vary with Newtonian fluids.

Fig. 4 elucidates the time independent-state U profiles for the variation of β and M against Y, respectively. It is seen that the U profile in this figure start with the no-slip boundary condition, reaches its peak and then shrinkages to zero along the Y coordinate satisfying the far-away boundary conditions. In the neighbourhood of the hot plate, it is noted that the magnitude of non-dimensional axial velocity (U) is amplifying as Y rises from $Y_{\min}$ ($=0$). Further, the time needed to achieve the steady-state upsurges as β and M increases. The time-independent U curves in the region near to the plate, i.e., $0 < Y < 2.6$ has decreasing trend for increasing values of β and Newtonian fluids ($\beta = 0$) is more than that of the couple stress fluids ($\beta > 0$), whereas opposite trend is noted in the region far from the hot plate, i.e., $Y > 2.6$. The similar observation is noted in the transient velocity Fig. 3(a) and (b).

4.2. Temperature

Fig. 5 depicts the variation of β and M on unsteady temperature profile (T) against the time (t) at the location (0, 0.35). From these data, in the beginning the unsteady temperature profile is found to drastically increase with time, reaches the peak value, then decreases and again slightly increases, and finally reached the time-independent state asymptotically. Also, it can be noted that for all transient T curves in the Fig. 5, the time to attain temporal peak upsurges as the non-dimensional parameter increases. It is observed from the Fig. 5 that, an upsurge in β or M results upsurge in the T profile. The reason behind this augmentation is an escalation in the fluid temperature implies an upsurge in the motion of fluid particles. The effective collision thus upsurges the motion of the fluid temperature near to the hot plate owing to decrease in the dynamic viscosity of the fluid. Also, it is clear that, the time-dependent temperature of the Newtonian fluid ($\beta = 0$) is less compared to the non-Newtonian couple stress fluid ($\beta > 0$).

Fig. 6 presents the steady-state non-dimensional T profiles versus the transverse coordinate for various values of β and M. These patterns begin with the boundary value of $T = 1$ and then reduce to zero. It is noted that, intensifying the β or M which ultimately results in rising the temperature. It is also pointed out that the time-independent state T curves have concurred with each other for different values of β as Y increases from 0 to 16. Therefore the effect of β on T curves has less impact compared to the U curves mentioned in Fig. 4. This is true since the

control parameters β appeared only in the momentum Eq. (11). Also, the steady-state temperature profiles of Newtonian fluids differ with non-Newtonian couple stress fluids.

4.3. Friction and heat transport coefficients

The momentum and heat transport coefficients are significant parameters in the heat

transfer studies due to their direct involvement in the convection. For the current problem, the non-dimensional average momentum and heat transport coefficients are defined as

$$\overline{C_f} = \int_0^1 \left(\frac{\partial U}{\partial Y}\right)_{Y=0} dX \tag{18}$$

$$\overline{Nu} = -\int_0^1 \left(\frac{\partial T}{\partial Y}\right)_{Y=0} dX \tag{19}$$

The above coefficients are calculated using 5-point approximation and Newton–Cotes quadrature formulae.

Figs. 7–8 illustrate the average skin-friction and heat transport coefficients against the time (t) covering various parametric values of β and M. Here, in this Fig. 7, at first the $\overline{C_f}$ increases with t, and after a certain lapse of time, they become independent of time throughout the transient period. Also, it is seen that $\overline{C_f}$ decreases with augmenting values of β or M. This is true and this is in line with the time-dependent velocity profile mentioned in Fig. 3(a). Fig. 8 illustrates that, in the beginning time, $\overline{Nu}$ decreases drastically, then slightly increasing and again reaches the time independent-state. Also, it is noted that initially the $\overline{Nu}$ curves coincided with each other and diverged after some time. More clearly, these figures show that in the starting time the heat conduction only occurs, and is dominant than the convection. Here it is perceived that $\overline{Nu}$ decreases with augmenting values of β or M as presented in Fig. 8, respectively. From the Fig. 7 it is identified that the average momentum transport coefficient of a couple stress fluid is less compared to the Newtonian fluid, and the same trend is noted for average heat transport coefficient which is shown in Fig. 8.

4.4. Entropy heat generation analysis and Bejan number

The entropy generation for couple stress fluid per unit volume with constant density given as [32,33,34,42]

$$S_{gen} = \frac{k}{T_\infty'^2}\left(\frac{\partial T'}{\partial y}\right)^2 + \left\{\frac{\mu}{T_\infty'}\left(\frac{\partial u}{\partial y}\right)^2 + \frac{\eta}{T_\infty'}\left(\frac{\partial^2 u}{\partial y^2}\right)^2\right\} + \frac{\sigma B_0^2 u^2}{T_\infty'} \tag{20}$$

Eq. (20) can be rewritten as

$$S_{gen} = S_1 + S_2 + S_3$$

where $S_1 = \frac{k}{T_\infty'^2}\left(\frac{\partial T'}{\partial y}\right)^2$, $S_2 = \frac{\mu}{T_\infty'}\left(\frac{\partial u}{\partial y}\right)^2 + \frac{\eta}{T_\infty'}\left(\frac{\partial^2 u}{\partial y^2}\right)^2$, $S_3 = \frac{\sigma B_0^2 u^2}{T_\infty'}$

Here S_1 signifies the entropy generation produced by heat flow, S_2 denotes the entropy generation due to viscous dissipation for a constant density couple stress fluid and S_3 signifies the entropy generation due to magnetic field.

The non-dimensional entropy heat generation parameter Ns is defined as the ratio of the volumetric entropy heat generation rate to the characteristic entropy heat generation rate. Accordingly, the entropy heat generation parameter is written as [43]

$$Ns = \left(\frac{\partial T}{\partial Y}\right)^2 + \frac{\mathrm{Br(Gr)}^2}{\Omega}\left\{\left(\frac{\partial U}{\partial Y}\right)^2 + \beta\left(\frac{\partial^2 U}{\partial Y^2}\right)^2\right\} + \frac{\mathrm{Br(Gr)}^2}{\Omega} M U^2 \tag{21}$$

where $\Omega = \frac{(T_w' - T_\infty')}{T_\infty'}$ is the non-dimensional temperature difference, and the characteristic entropy heat generation is $\frac{k(T_w' - T_\infty')^2}{T_\infty'^2 l^2}$. The Eq. (21) can be rewritten in the following form

$$N_S = N_1 + N_2 + N_3 \tag{22}$$

where $N_1 = \left(\frac{\partial T}{\partial Y}\right)^2$, $N_2 = \frac{\mathrm{Br(Gr)}^2}{\Omega}\{\left(\frac{\partial U}{\partial Y}\right)^2 + \beta\left(\frac{\partial^2 U}{\partial Y^2}\right)^2\}$ and $N_2 = \frac{\mathrm{Br(Gr)}^2}{\Omega} M U^2$ designate the irreversibility owing to heat transfer, fluid friction (viscous dissipation) and magnetic field effect, respectively.

To assess the irreversibility distribution, the parameter *Be* (Bejan number) is defined as the ratio of entropy heat generation due to heat

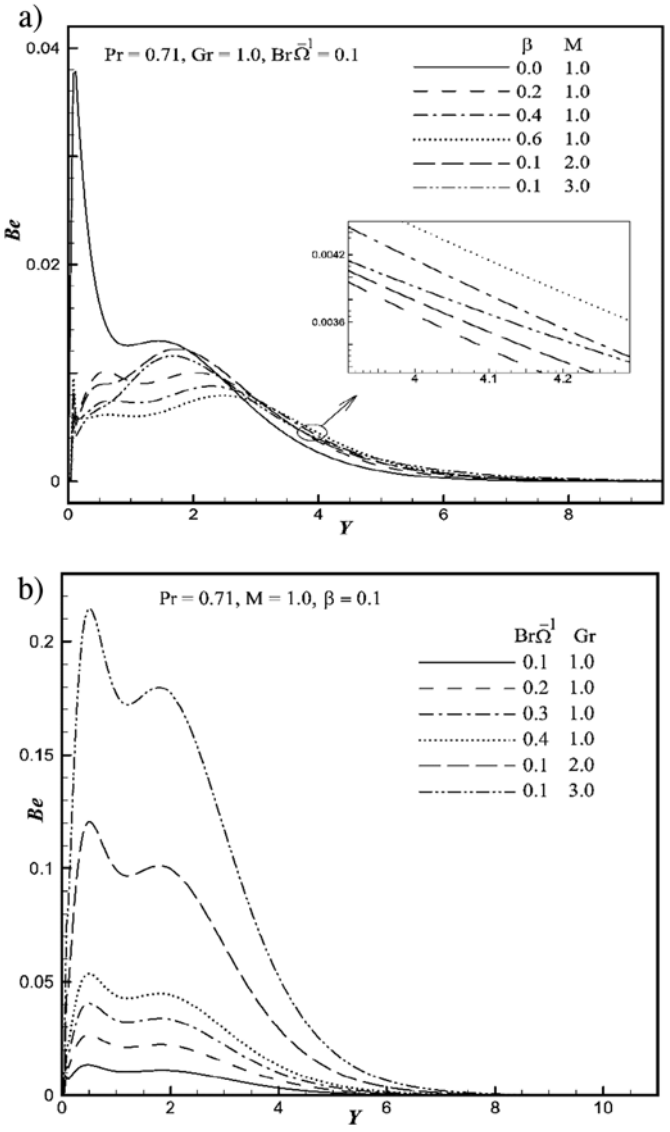

Fig. 11. Simulated steady-state Bejan profile (*Be*) versus *Y* at $X = 1.0$ for distinct values of (a) β and M; & (b) $\mathrm{Br}\Omega^{-1}$ and *Gr*.

transfer to the overall entropy heat production Eq. (22), and is given by

$$Be = \frac{N_1}{N_1 + N_2 + N_3} \tag{23}$$

From Eq. (23), it is understood that the Bejan number lies between 0 and 1 i.e. $0 \le Be \le 1$. Consequently, $Be = 0$ reveals that the parameters N_2 and N_3 dominates the parameter N_1, whereas $Be = 1$ indicates that the parameter N_1 dominates the parameters N_2 and N_3. It is obvious that at $Be = 0.5$, the contribution of fluid friction and magnetic field in the entropy generation production is equal to irreversibility due to heat transfer i.e. $N_2 + N_3 = N_1$.

The simulated time-independent dimensionless *Ns* profile for different control parameters β, M, $Br\Omega^{-1}$ and *Gr* along the transverse direction at $X = 1.0$ are revealed in Fig. 9(a)–(b), respectively. It is remarked that as the *Y* coordinate increases, the *Ns* curves drastically increases and achieves the peak value, then suddenly decreases and reaches monotonically to zero. Also, it is identified that the entropy production gets thinner boundary layer for all values of control parameters. This is as a result of higher entropy production is observed adjacent to the plate which yields thinner boundary layer. Fig. 9(a) represents the effect of β and M on *Ns*. From this plot, it is perceived that for augmenting values of β and M, the steady-state *Ns* curves decreases near to the plate (i.e., in the interval $Y \in [0, 3.6]$), then increases when $Y > 3.6$. This is because of reduction in the heat transport coefficient near to tropical region causes decrease in *Ns* (Refer Fig. 8). Also, from the Fig. 9(a) it is perceived that the entropy production near to the plate (i.e., $0 < Y < 2.78$) for couple stress fluid is less in comparison with that of a Newtonian fluid and the opposite tendency is seen when $Y > 2.78$. Fig. 9(b) reveals that the entropy increases in the vicinity of a hot plate, then it decreases drastically, and approach to zero along the *Y* coordinate. It is also noted that for augmenting values of $Br\Omega^{-1}$ and *Gr*, the *Ns* curves increases. The reason behind this statement is, for larger values of Grashof number or group parameter, the entropy production due to the fluid friction increases.

Fig. 10(a)–(d) represent the entropy lines for various values of couple stress parameter (β), group parameter ($Br\Omega^{-1}$), magnetic parameter (M) and Grashof number (*Gr*), respectively. Here in these figures it is observed that the entropy lines occur in the neighbourhood of hot wall plate for all values of control parameters. From Fig. 10(a), (b) and (d) it is seen that, at any point of location (*X*,*Y*) the entropy contour value increases for increasing values of β, $Br\Omega^{-1}$ & *Gr* and the opposed trend is noticed for values of M which is depicted in Fig. 10(c). Also, near the leading edge of the plate the entropy contours show lower values for β, M and *Gr* as compared to $Br\Omega^{-1}$. This is true since the entropy production is less for β, M and *Gr* near to leading edge of the plate as compared to $Br\Omega^{-1}$. Finally, it is noted that the deviation of entropy lines from the hot plate is less for increasing values of β and M as compared to *Gr* and $Br\Omega^{-1}$.

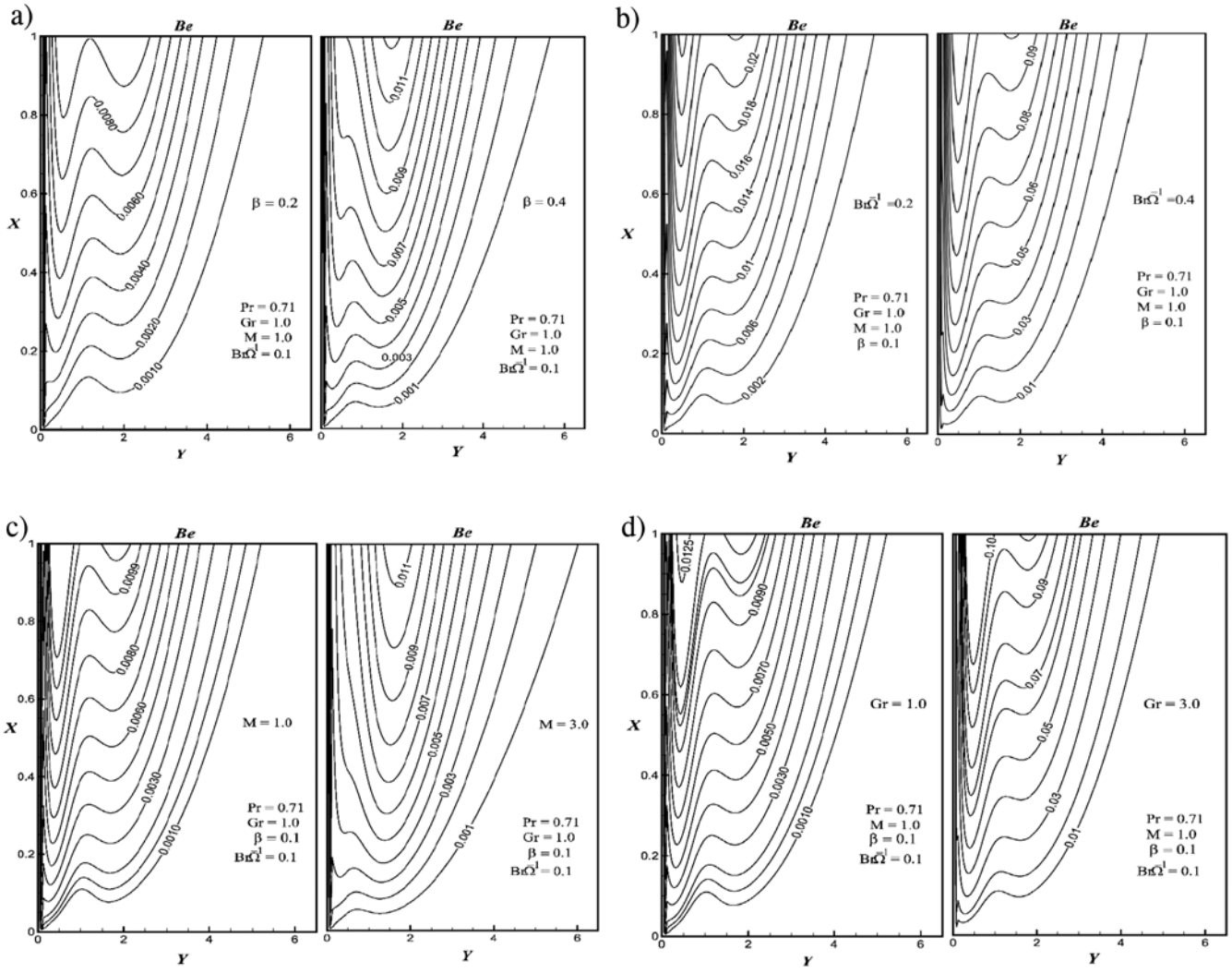

Fig. 12. Simulated steady-state Bejan lines (*Be*) for distinct values of (a) β; (b) $Br\Omega^{-1}$; (c) M; & (d) Gr.

Fig. 11 demonstrates the time-independent state *Be* against the transverse direction at $X = 1.0$ for various parameter values. The effects of β, M, $Br\Omega^{-1}$ and Gr on *Be* are shown in Fig. 11(a)–(b), respectively. Here in all these figures, the steady-state characteristics of Bejan number are almost similar to time-independent state entropy generation (*Ns*) which is shown in the Fig. 9(a)–(b). Overall it is seen that the steady-state *Be* decreases as β or M upsurges in the *Y* coordinate interval i.e., $Y \in (0, 2.8)$ and the reverse trend is obtained when $Y > 2.8$. Also, the time-independent state *Be* upsurges for increasing values of $Br\Omega^{-1}$ and *Gr*. The important observation from these figures is, the steady-state entropy production is more than the Bejan number near the wall. This confirms that smaller *Be* yields an increase in N_2, i.e., $N_1 < N_2$ (Refer Eq. (23)) and thus irreversibility due to heat transfer is dominated by fluid friction which gives more entropy production in the vicinity of plate. Also from the Fig. 11(a) it is remarked that the Bejan number is high for Newtonian fluid compared to the couple stress fluid.

Fig. 12(a)–(d) illustrate the Bejan lines for different values of β, $Br\Omega^{-1}$, M and *Gr*, respectively. Here in all these figures the Bejan lines have different trend for all control parameters as compared to entropy lines which is shown in Fig. 10(a)–(d). It is observed that in the 2D rectangular coordinate system i.e. $0 < X \le 1, 0, \quad 0 < Y \le 2$, the Bejan lines have more fluctuation as compared to entropy lines. Further, in the vicinity of the hot plate it is identified that, for all values of β, the Bejan lines are adhering to the plate, whereas these lines tend to move away from the plate for the control parameters M, *Gr* and $Br\Omega^{-1}$ as *Y* increases. Also, the important observation from these figures is the Bejan lines occur only in the proximity of the hot vertical plate. Finally, it is concluded that the Bejan lines move away from the hot wall for all increasing values of control parameters.

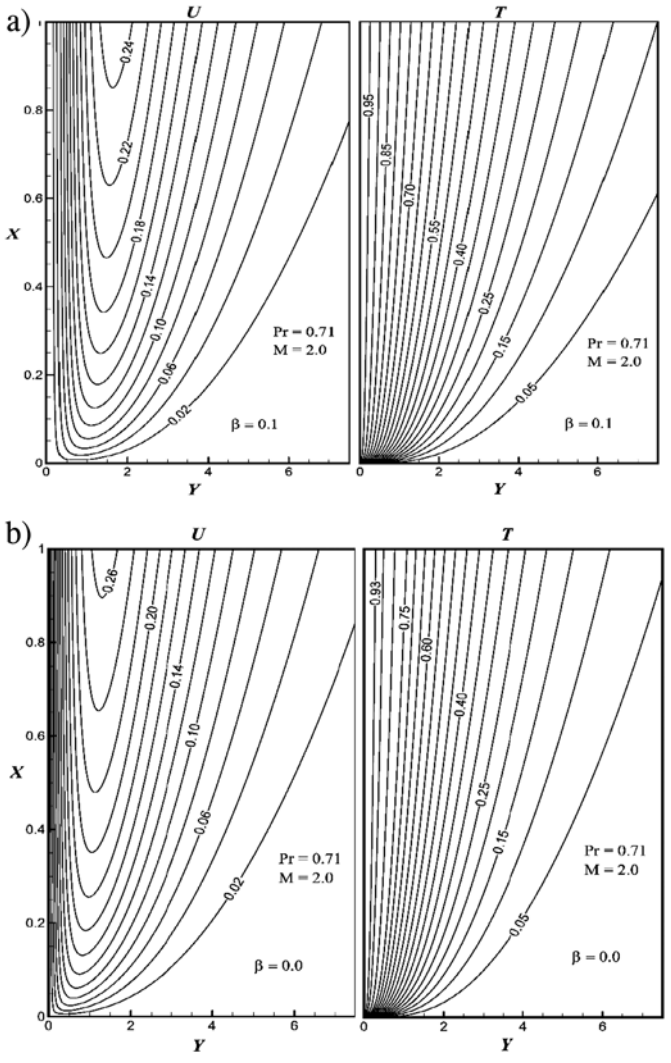

Fig. 13. Time-independent state contours of velocity (*U*) and temperature (*T*) for (a) couple stress fluid ($\beta = 0.1$); & (b) Newtonian fluid ($\beta = 0.0$).

4.5. Differences between couple stress and Newtonian fluid flows

Fig. 13 elucidates the flow-field variable contours for couple stress and Newtonian fluid flows. Fig. 13(a) represents couple stress fluid and Fig. 13(b) for Newtonian fluid. Here the velocity of the couple stress fluid flow is observed to be less compared to the Newtonian fluid flow, but with respect to the temperature the opposite trend is observed. Also, the time independent state temperature contours for couple stress fluid are slightly different, with thicker temperature boundary layer, from that of the Newtonian fluid.

5. Concluding remarks

In this work, the entropy heat generation distribution for time-dependent couple stress fluid flow past a vertical plate is discussed numerically. The finite difference method is applied to solve the mathematical flow-field equations with the aid of Thomas and pentadiagonal algorithms. The entropy heat generation and Bejan number distributions are derived and evaluated with the help of flow variables. The influences of couple stress and magnetic field parameter on flow distributions along with average heat and momentum transport coefficients are discussed. Further, the effect of couple stress parameter, magnetic parameter, group parameter and Grashof number on entropy heat generation and Bejan number are analyzed. Also, results from this article could be useful for experimental studies which are related to blood flows, colloidal solutions, lubrication theory, seawater propulsion, energy minimization etc. Few important conclusions are listed below:

1. The time taken to achieve the steady-state amplifies for the augmenting values of couple stress parameter and magnetic parameter.
2. The velocity decreases and temperature increases with rising values of β or M. Also $\overline{C_f}$ and $\overline{Nu}$ decreases with augmenting values of β or M.
3. Entropy heat generation parameter and Bejan number decrease for cumulative values of β or M. While the trend is inverted for Grashof number and group parameter.
4. The transient and steady-state results of flow variables, average heat and momentum transport coefficients for non-Newtonian couple stress fluid differs with Newtonian fluids.
5. The entropy and Bejan contour value decreases for increasing values of β and $Br\Omega^{-1}$.

Acknowledgements

The second author Mahesh Kumar wishes to thank DST-INSPIRE (Code No. IF160028) for the grant of research fellowship and to Central University of Karnataka for providing the research facilities.

References

[1] A. Acrivos, A theoretical analysis of laminar natural convection heat transfer to non-Newtonian fluids, A.1.Ch.E. J. 4 (1960) 584–590.
[2] H.T. Chen, C.H. Chen, Free convection flow of non-Newtonian fluids along a vertical plate embedded in a porous medium, J. Heat Transf. 110 (1988) 257–260.
[3] A.J. Chamkha, A.M. Aly, M.A. Mansour, Unsteady natural convective power-law fluid flow past a vertical plate embedded in a non-Darcian porous medium in the presence of a homogeneous chemical reaction, Nonlinear Anal. Model. Control 15 (2010) 139–154.
[4] V.R. Prasad, S.A. Gaffar, K.E. Reddy, O.A. Bég, S. Krishnaiah, A mathematical study for laminar boundary-layer flow heat and mass transfer of a Jeffrey non-Newtonian fluid past a vertical porous plate, Heat Transf. Asian Res. 44 (2013) 189–210.
[5] A. Hussanan, M.Z. Salleh, R.M. Tahar, I. Khan, Unsteady boundary layer flow and heat transfer of a Casson fluid past an oscillating vertical plate with Newtonian heating, PLoS ONE 9 (2014) (e108763).

[6] A. Pantokratoras, Natural convection over a vertical isothermal plate in a non-Newtonian power-law fluid: new results, Adv. Mech. Eng. 8 (2016) 1–12.
[7] V.K. Stokes, Couple stresses in fluids, Phys. Fluids 9 (1966) 1709–1715.
[8] N.B. Naduvinamani, A. Siddangouda, Effect of surface roughness on the hydrodynamic lubrication of porous step-slider bearings with couple stress fluids, Tribol. Int. 40 (2007) 780–793.
[9] K.C. Valanis, C.T. Sun, Poiseuille flow of a fluid with couple stress with applications to blood flow, Biorheology 6 (1969) 85–97.
[10] G. Ramanaiah, P. Sarkar, Squeeze films and thrust-bearings lubricated by fluids with couple stress, Wear 48 (1978) 309–316.
[11] L.M. Srivastava, Flow of couple stress fluid through stenotic blood-vessels, J. Biomech. 18 (1985) 479–486.
[12] R.S. Gupta, L.G. Sharma, Analysis of couple stress lubricant in hydrostatic thrust bearings, Wear 48 (1988) 257–269.
[13] M. Devakar, T.K.V. Iyengar, Run up flow of a couple stress fluid between parallel plates, Nonlinear Anal. Model. Control 15 (2010) 29–37.
[14] N.A. Khan, F. Riaz, N.A. Khan, Heat transfer analysis for couple stress fluid over a nonlinearly stretching sheet, Nonlinear Eng. 2 (2013) 121–127.
[15] S. Akhtar, Flows between two parallel plates of couple stress fluids with time-fractional Caputo and Caputo-Fabrizio derivatives, Eur. Phys. J. Plus 131 (2016) 401–413.
[16] E.M. Korchevskii, L.S. Marochnik, Magnetohydrodynamic version of movement of blood, Biophysics 10 (1965) 411–413.
[17] G. Herdrich, M. Auweter-Kurtz, M. Fertig, A. Nawaz, D. Petkow, MHD flow control for plasma technology applications, Vacuum 80 (2006) 1167–1173.
[18] D.O. Gomez, P.D. Mininni, Direct numerical simulations of helical dynamo action: MHD and beyond, Nonlinear Process. Geophys. 11 (2004) 619–629.
[19] P. Graneau, Electrodynamic seawater jet: an alternative to the propeller? IEEE Trans. Magn. 25 (1989) 3275–3277.
[20] A. Tsinober, MHD flow drag reduction, in viscous drag reduction in boundary layers, in: D.M. Bushnell, J.N. Hefner (Eds.),Prog. Astron. Aeron., Vol. 123, 1990, pp. 327–349.
[21] S. Rashidi, M. Bovand, J.A. Esfahani, Application of magnetohydrodynamics for suppressing the fluctuations in the unsteady flow around two side-by-side circular obstacles, Eur. Phys. J. Plus vol. 131 (2016) 423.
[22] S. Rashidi, J.A. Esfahani, M. Maskaniyan, Applications of magnetohydrodynamics in biological systems-a review on the numerical studies, J. Magn. Magn. Mater. 439 (2017) 358–372.
[23] R. Muthuraj, S. Srinivas, R.K. Selvi, Heat and mass transfer effects on MHD flow of a couple-stress fluid in a horizontal wavy channel with viscous dissipation and porous medium, Heat Transf. Asian Res. 42 (2013) 403–421.
[24] A. Nayak, G.C. Dash, Magnetohydrodynamic couple stress fluid flow through a porous medium in a rotating channel, J. Eng. Thermophys. 24 (2015) 283–295.
[25] S. Ravi Kumar, Effect of couple stress fluid flow on magnetohydrodynamic peristaltic blood flow with porous medium through inclined channel in the presence of slip effect-blood flow model, Int. J. Bio-Sci. Bio-Technol. 7 (2015) 65–84.
[26] D. Srinivasacharya, G. Madhava Rao, Computational analysis of magnetic effects on pulsatile flow of couple stress fluid through a bifurcated artery', Comput. Methods Prog. Biomed. 137 (2016) 269–279.
[27] N.A. Khan, H. Khan, S.A. Ali, Exact solutions for MHD flow of couple stress fluid with heat transfer, J. Egypt. Math. Soc. 24 (2016) 125–129.
[28] N. Ali, S. Ullah Khan, M. Sajid, Z. Abbas, MHD flow and heat transfer of couple stress fluid over an oscillatory stretching sheet with heat source/sink in porous medium, Alex. Eng. J. 55 (2016) 915–924.
[29] G. Giangaspero, E. Sciubba, Application of the entropy generation minimization method to a solar heat exchanger: a pseudo-optimization design process based on the analysis of the local entropy generation maps, Energy 58 (2013) 52–65.
[30] V. Badescu, Optimal paths for minimizing lost available work during usual heat transfer processes, J. Non-equilib. Thermodyn. 29 (2004) 53–73.
[31] H. Kockum, A. Jernqvist, Entropy generation in multifield flows: equations and examples of applications, Inst. Chem. Eng. Trans. IChemE 76 (1998) 212–222.
[32] G. Nagaraju, J. Srinivas, J.V. Ramana Murthy, A.M. Rashad, Entropy generation analysis of the MHD flow of couple stress fluid between two concentric rotating cylinders with porous lining, Heat Transf. Asian Res. 46 (2016) 316–330.
[33] S.O. Kareem, S.O. Adesanya, J.A. Falade, U.E. Vincent, Entropy generation rate in unsteady buoyancy-driven hydromagnetic couple stress fluid flow through a porous channel, Int. J. Pure Appl. Math. 115 (2017) 311–326.
[34] S.O. Kareem, S.O. Adesanya, U.E. Vincent, Second law analysis for hydromagnetic couple stress fluid flow through a porous channel, Alex. Eng. J. 55 (2016) 925–931.
[35] J.V. Ramana Murthy, J. Srinivas, First and second law analysis for the mhd flow of two immiscible couple stress fluids between two parallel plates, Heat Transf. Asian Res. 44 (2015) 468–487.
[36] Y. Aksoy, Effects of couple stresses on the heat transfer and entropy generation rates for a flow between parallel plates with constant heat flux, Int. J. Therm. Sci. 107 (2016) 1–12.
[37] J. Srinivas, J.V. Ramana Murthy, O.A. Bég, Entropy generation analysis of radiative heat transfer effects on channel flow of two immiscible couple stress fluids, J. Braz. Soc. Mech. Sci. Eng. 39 (2017) 2191–2202.
[38] H.P. Rani, G. Janardhana Reddy, C.N. Kim, Y. Rameshwar, Transient couple stress fluid past a vertical cylinder with Bejan's heat and mass flow visualization for steady-state, ASME J. Heat Transf. 137 (2015) 1–12.
[39] V.K. Stokes, Theories of Fluids with Microstructure, Springer-Verlag, New York, Tokyo, 1984.
[40] H. Schlichting, Boundary Layer Theory, 6th edition McGraw-Hill, New York, 1968.
[41] H.S. Takhar, P. Ganesan, K. Ekambavanan, V.M. Soundalgekar, Transient free convection past a semi-infinite vertical plate with variable surface temperature, Int. J. Numer. Methods Heat Fluid Flow 7 (1997) 280–296.
[42] A.J. Chamkha, A.M. Rashad, M.A. Mansour, T. Armaghani, M. Ghalambaz, Effects of heat sink and source and entropy generation on MHD mixed convection of a Cu-water nanofluid in a lid-driven square porous enclosure with partial slip, Phys. Fluids 29 (2017) 052001.
[43] A. Bejan, Entropy Generation Minimization, CRC Press, New York, 1996.